Liquid Crystals
Publication details, including instructions for authors and subscription information:
http://www.informaworld.com/smpp/title~content=t713926090

Ferroelectric and antiferroelectric modes in a new chiral thiobenzoate liquid crystal

P. Simeão Carvalho[a]; M. R. Chaves[a]; C. Destrade[b]; Huu Tinh Nguyen[b]; M. Glogarová[c]
[a] Laboratório de Física, Faculdade de Ciĕncias da Universidade do Porto, Porto, Portugal [b] Centre de Recherche Paul Pascal, Pessac, France [c] Institute of Physics, Academy of Sciences of the Czech Republic, Prague, Czech Republic

To cite this Article Carvalho, P. Simeão , Chaves, M. R. , Destrade, C. , Nguyen, Huu Tinh and Glogarová, M.(1996) 'Ferroelectric and antiferroelectric modes in a new chiral thiobenzoate liquid crystal', Liquid Crystals, 21: 1, 31 — 37
To link to this Article: DOI: 10.1080/02678299608033793
URL: http://dx.doi.org/10.1080/02678299608033793

LIQUID CRYSTALS, 1996, VOL. 21, NO. 1, 31-37

Ferroelectric and antiferroelectric modes in a new chiral thiobenzoate liquid crystal

by P. SIMEÃO CARVALHO*†, M. R. CHAVES†, C. DESTRADE‡, HUU TINH NGUYEN‡ and M. GLOGAROVÁ§

†Laboratório de Física, Faculdade de Ciências da Universidade do Porto, Ruado Campo Alegre, 687, 4150, Porto, Portugal

‡Centre de Recherche Paul Pascal, Av. Schweitzer, 33600 Pessac, France

§Institute of Physics, Academy of Sciences of the Czech Republic, Na Slovance 2, 18040, Prague 8, Czech Republic

(*Received 10 July 1995; in final form 14 October 1995; accepted 24 October 1995*)

This work concerns the dielectric relaxation study of a new compound containing a thiobenzoate group with a fluoro substituent, which presents a sequence of antiferro-, ferri-, ferroelectric and $S^*_{C_\alpha}$ phases. The polar character of these phases was confirmed by optical hysteresis loops. Three modes with a nearly monodispersive behaviour were identified: the soft mode, the Goldstone mode and a non-collective azimuthal mode. The soft mode softens above the $S_A - S^*_{C_\alpha}$ transition and triggers another mode within the $S^*_{C_\alpha}$ phase. Moreover, a collective anti-phase azimuthal mode appears and may be the origin of the onset of the antiferroelectric $S^*_{C_A}$ phase. A strong influence of surface interactions on the thermal hysteresis and on the dielectric constant was evident in this work.

1. Introduction

Recently, new liquid crystals containing a thiobenzoate group [1, 2] were synthesized which exhibit antiferro-, ferri- and ferro-electric mesophases. The new compound studied here has a thiobenzoate group with fluoro substituent and the chemical formula is

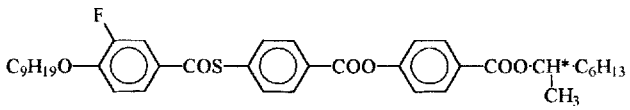

Between the crystal (Cr) and the isotropic (I) phase, this compound presents the following sequence of phases:

Cr 87°C $S^*_{C_A}$ 93°C $S^*_{C_{FI}}$ 98°C S^*_C 103·9°C $S^*_{C_\alpha}$ 105·7°C S_A 135°C I

The transition temperatures were determined by differential scanning calorimetry (DSC) measurements with increasing temperatures and by optical microscopic texture observations. The phase sequence assignment was assessed by analogy with results from studies of other compounds with similar formulae [1].

In this work, we present some optical hysteresis loops and a dielectric relaxation study of all the phases. Several relaxation modes were identified whose contributions to the complex dielectric constant seem to depend on the samples thickness.

*Author for correspondence.

2. Experimental

This study was made on samples 7·5 μm (sample 1) and 25 μm (sample 2) thick. The cells, produced commercially by Linkam Scientific Instruments Ltd were filled by capillary action. All the measurements on heating and cooling runs were done between the isotropic and the $S^*_{C_A}$ phases, without going into the crystalline phase. The alignment of the liquid crystal was evaluated by optical observations.

The complex dielectric constant ($\varepsilon', \varepsilon''$) was measured with a HP4284A LCR Meter, at stabilized temperatures. The temperature was measured by a chromel–alumel thermocouple and controlled by a Macintosh computer, with an accuracy better than 0·05°C. The range of the measuring frequencies was 20 Hz–1 MHz.

The optical hysteresis loops were obtained on heating runs by measuring the transmitted light intensity I with a PIN Hamamatsu photodiode, attached to a polarizing microscope. A halogen lamp was used as a light source and the temperature was controlled by a Mettler FP90 oven. The applied electric field was a triangular wave at a frequency between 0·6 Hz ($S^*_{C_A}$ phase) and 17 Hz (S_A phase).

The temperature dependence of the transmitted light was measured for heating and cooling runs at a rate of $0{\cdot}3^{\circ}C\,min^{-1}$. For the detection of the transmitted light we used a BPW21 photodiode from R. S. Components Ltd (spectral banwidth between 440 nm and 680 nm) and the light source was a He–Ne laser (632·8 nm).

3. Results and discussion

3.1. *Identification of phases*

The existence of several smectic polar phases in sample 1 (7·5 μm thick) was confirmed by the detection of the transmitted light intensity as a function of the electric field $I(E)$, at different temperatures. Figure 1 depicts some optical hysteresis loops for sample 1, obtained at a stabilized temperature on heating, after cooling from the isotropic phase without going into the crystalline phase. The shape of the loops shows the existence of antiferro-($S^*_{C_A}$), ferro-(S^*_C), ferri-electric ($S^*_{C_{FI}}$) and $S^*_{C_\alpha}$ phases.

Although DSC measurements on heating indicate a transition between the crystalline phase and the S^*_{CA} phase at 87°C, on cooling this transition occurs at ≈67°C, which is due to the well-known supercooling phenomenon. This explains why at 72°C a double hysteresis loop can be seen with a threshold field of about $0{\cdot}6\,V\,\mu m^{-1}$, corresponding to the $S^*_{C_A}$ phase. The peaks

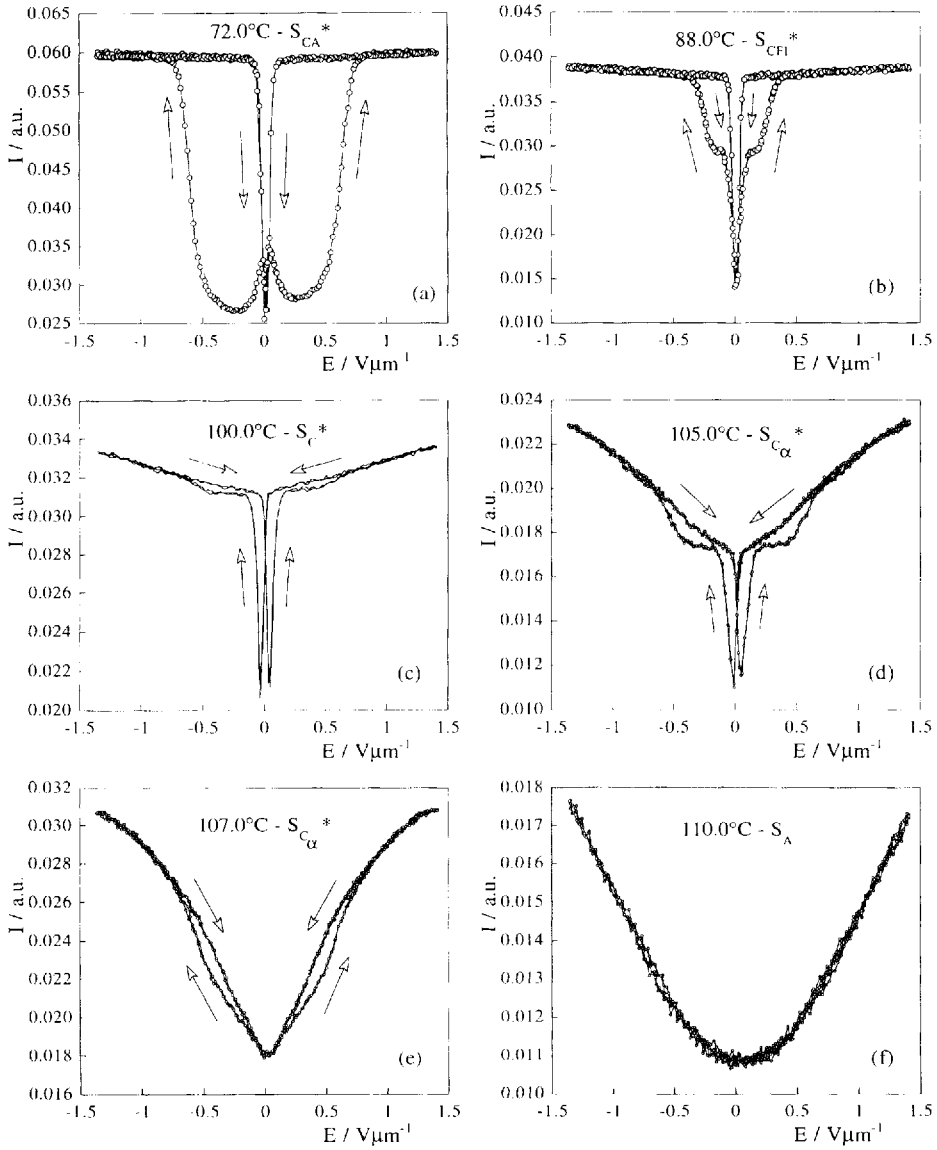

Figure 1. Transmitted light $I(E)$ for sample 1. The Loops were obtained for the (*a*) $S^*_{C_A}$, (*b*) $S^*_{C_{FI}}$, (*c*) S^*_C, (*d*), (*e*) $S^*_{C_\alpha}$ and (*f*) S_A phases, at the temperatures indicated.

observed at zero field are due to ferroelectric switching which takes place only near the surfaces. This effect disappears on lowering the frequency.

At 88°C the threshold field is no longer detected and the double hysteresis loop corresponds to the induced transition from the ferrielectric to the ferroelectric saturated state. With the thin sample the S^*_{CA}–S^*_{CFI} transition, as well as the S^*_{CFI}–S^*_C transition, occurs at *lower* temperatures than those found by DSC heating measurements. The latter technique reveals mainly bulk properties. In the $S^*_{C\alpha}$ phase, the shape of the loop changes progressively from a S^*_C-like (105°C) to a S_A-like (107°C) loop. The upper limit of the temperature range of the $S^*_{C\alpha}$ phase is slightly higher than that found by DSC measurements, which may be due to different oven temperature calibrations.

In sample 2 (2·5 μm thick), the study of these smectic phases was made by measuring the transmitted light intensity as a function of the temperature, $I(T)$. Several anomalies can be seen in figure 2, some of them corresponding to phase transitions. The curves were obtained from heating and cooling runs as indicated by the arrows. A thermal hysteresis can be observed for the S^*_C–S^*_{CFI} and S^*_{CFI}–S^*_{CA} phase transition temperatures, but the temperature range of stability of the S^*_{CFI} phase does not change significantly. The S_A–$S^*_{C\alpha}$ phase transition is not clearly observed.

We must point out that the transition temperatures found for sample 2 (25 μm thick) on heating are in agreement with the temperatures found from DSC measurements, in contrast to those observed for the thinner sample 1 (7·5 μm thick). This behaviour may be due to an influence of the surface on the stabilization of the ferroelectric phase relative to the ferrielectric phase, and of the ferrielectric phase relative to the antiferroelectric phase.

Dielectric measurements, performed on both samples, show a dielectric dispersion in all the phases. The real dielectric constant ε' exhibits a maximum between ≈103°C and ≈110°C, but the temperature at which that maximum occurs depends on the measuring frequency. Such a behaviour was earlier observed for another compound with a similar chemical formula [3]. Figure 3 shows ε' at 20 Hz for samples 1 and 2. Here, we have clear evidence for a thermal hysteresis, but much more explicitly in the thinner sample (sample 1) than in the thicker sample (sample 2). The arrows indicate the heating and the cooling runs. The sharp decrease in the dielectric constant at low temperature corresponds to the lower limit of the ferroelectric S^*_C phase.

The S^*_{CFI} phase can be identified in sample 2 by a step in ε', which is not observed in sample 1. For the heating runs, the lower limit of the S^*_C phase is located at the same temperature for both samples (≈96°C), so the thermal hysteresis only occurs within the S^*_{CA} and the S^*_{CFI} phases.

In the S^*_{CA} phase, the samples probably retain ferroelectric layers near the surfaces due to preferred polar anchoring at the surfaces. These layers, which have a definite thickness determined by the anchoring strength, contribute to the dielectric constant, the effective contribution being higher in thin samples.

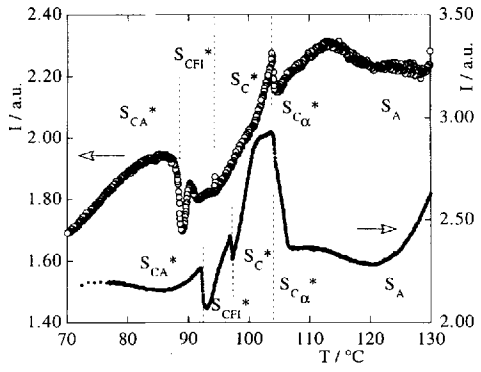

Figure 2. Transmitted light intensity $I(T)$ for sample 2 at zero electric field, for a heating run (●) and for a cooling run (○).

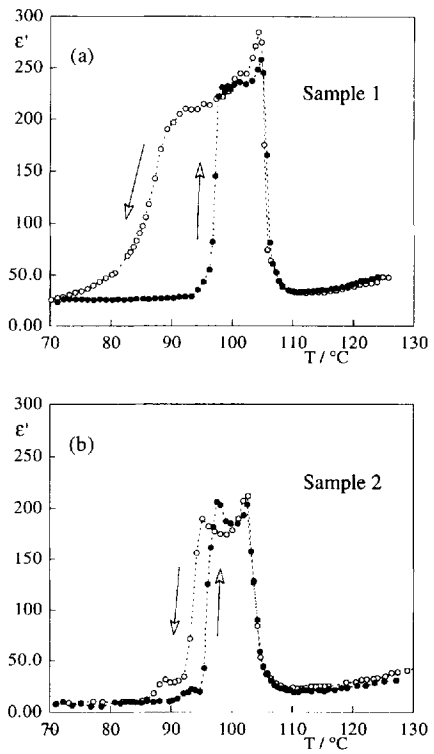

Figure 3. Temperature dependence of the dielectric constant (*a*) for sample 1 and (*b*) for sample 2, for heating (●) and cooling (○) runs.

3.2. *Dielectric relaxation study*

It is known from the literature [4] that ionic conduction and the relaxation modes make considerable contributions to the complex dielectric constant. If different relaxation modes coexist at a given temperature, it is assumed that the complex dielectric constant reflects the contributions and the coupling between these modes. In this study, we have considered three parameters that give important information about the relaxation modes. These parameters are: $\Delta\varepsilon$ (the relaxation amplitude, defined as $\Delta\varepsilon=\varepsilon(0)-\varepsilon(\infty)$), β (a Cole–Cole parameter that reflects the polydispersive behaviour of the mode; $\beta=1$ corresponds to a monodispersive relaxation mode) and f_r (the relaxation frequency). $\Delta\varepsilon$ and β were calculated from Cole–Cole fits to the complex dielectric constant $\varepsilon^*=(\varepsilon',\varepsilon'')$. The relaxation frequencies $f_r=1/2\pi\tau$ were obtained from the maxima of $\varepsilon''(f)$. By assuming that $\varepsilon^*(\omega)$ is the sum of different contributions and that each mode obeys a Cole–Cole relaxation [4], we have

$$\varepsilon^*(\omega)=\varepsilon(\infty)+\sum_n \frac{\Delta\varepsilon_n}{1+(j\omega\tau_n)^{\beta n}}, \quad \begin{matrix} 0<\beta<1 \\ n=1;\ 2;\ldots \end{matrix}$$

when n labels each mode. For simplicity, we shall analyse the data obtained from the *cooling runs*, although data corresponding to the heating runs were also studied. The values obtained for $\Delta\varepsilon$, β and f_r were very similar for increasing and decreasing temperatures.

In figure 4, the temperature dependences of $1/\Delta\varepsilon$, β and f_r for sample 1 and for sample 2 are displayed for the relaxation processes found in the temperature interval studied.

In the S_A phase, only one relaxation mode is observed. Taking into account the molecular structure of the S_A phase, this mode must correspond to the *amplitude mode* [5] (so-called *soft mode*) which is associated with fluctuations of the molecular tilting and has a quasi-monodispersive behaviour in the S_A phase. When approaching the S_A–$S^*_{C_\alpha}$ phase transition (at $\approx 107°C$), its relaxation frequency decreases sharply and the relaxation amplitude $\Delta\varepsilon$ increases. The parameter β, associated with the distribution of the relaxation times of this mode, decreases as shown in figure 4 (*c*) and 4 (*d*). The relaxation frequency and the dielectric amplitude of the soft mode depend on the sample thickness. For the thin sample (see figure 4 (*a*)), $\Delta\varepsilon$ as well as the relaxation frequency are higher than that for the thick sample (see figure 4 (*d*)). Similar results for the thickness dependence of the relaxation frequency has been found in [6] and the effect can be attributed to a change in the elastic properties due to surface interactions.

In the tilted phases, the analysis of $\varepsilon^*(T)$ discloses three relaxation processes, RP1, RP2 and RP3, as shown in figure 4. Each relaxation process takes place in different frequency ranges. RP1 occurs at a low frequency range, RP3 at a high frequency range and RP2 in between. Figure 5 shows the contributions of these relaxation processes in the S^*_C phase, expressed by Cole–Cole diagrams. The detection of these modes was limited by the experimental accuracy.

In the $S^*_{C_\alpha}$ phase, the relaxation process denoted as RP2 exhibits an increasing contribution of $\Delta\varepsilon$ and a decreasing contribution of f_r when decreasing the temperature. However, RP2 can not be taken as the amplitude mode, which occurs in the S_A phase and gives its maximum contribution to ε^* at the S_A–$S^*_{C_\alpha}$ transition temperature. We suppose that the mode corresponding to RP2 is triggered by the amplitude mode in the vicinity of the S_A–$S^*_{C_\alpha}$ transition temperature. This triggered mode gives a maximum contribution to the permittivity at the $S^*_{C_\alpha}$–S^*_C transition temperature; therefore it should be associated with the $S^*_{C_\alpha}$ phase and the onset of the $S^*_{C_\alpha}$–S^*_C transition. RP2 has been detected in the S^*_C phase and in the $S^*_{C_{FI}}$ phase only for sample 1 (7·5 μm thick). Its origin is not understood.

RP1 has a very high $\Delta\varepsilon$ and a nearly constant $f_r \approx 300$ Hz in the S^*_C phase for sample 2. In sample 1, the relaxation frequency f_r could not be determined due to the ionic contribution to ε''. In the literature, it is usual to associate the strongest contribution to $\Delta\varepsilon$ in the S^*_C phase with the precessing of the tilted molecules around the helicoidal axis [4, 5] (the *phason mode*, also called the *Goldstone mode*). The mode corresponding to RP1 in the $S^*_{C_\alpha}$, S^*_C and $S^*_{C_{FI}}$ phases seems to be such a mode. In the $S^*_{C_\alpha}$ phase, the contribution of this mode to the permittivity increases strongly with decreasing temperature; this can be a consequence of the pitch increase as similarly reported [3] and [7].

In the $S^*_{C_{FI}}$ phase, where the local polarization is partially compensated, the contribution from the Goldstone mode to $\Delta\varepsilon$ is lower than that in the S^*_C phase. In the $S^*_{C_A}$ phase, the polarization is fully compensated and no contribution from this mode should be found. However, a relaxation process in the same frequency range as that of RP1, was observed in the $S^*_{C_A}$ phase. The temperature dependence of $\Delta\varepsilon$ in this phase suggests that this relaxation process in the $S^*_{C_A}$ phase can have the same origin as that considered by Gisse *et al.* [7], to describe the dielectric behaviour in the ferrielectric and antiferroelectric phases in terms of variation of the angle ψ between the molecules in neighbouring layers (designated as anti-phase azimuthal mode). As was pointed out in [7], this mode is decisive for the onset of the $S^*_{C_A}$–$S^*_{C_{FI}}$ phase transition and should also be active just above this transition, in the $S^*_{C_{FI}}$ phase. It is probable that, in this range, the anti-phase azimuthal mode is mixed with the Goldstone mode, as the relaxation frequencies of both modes

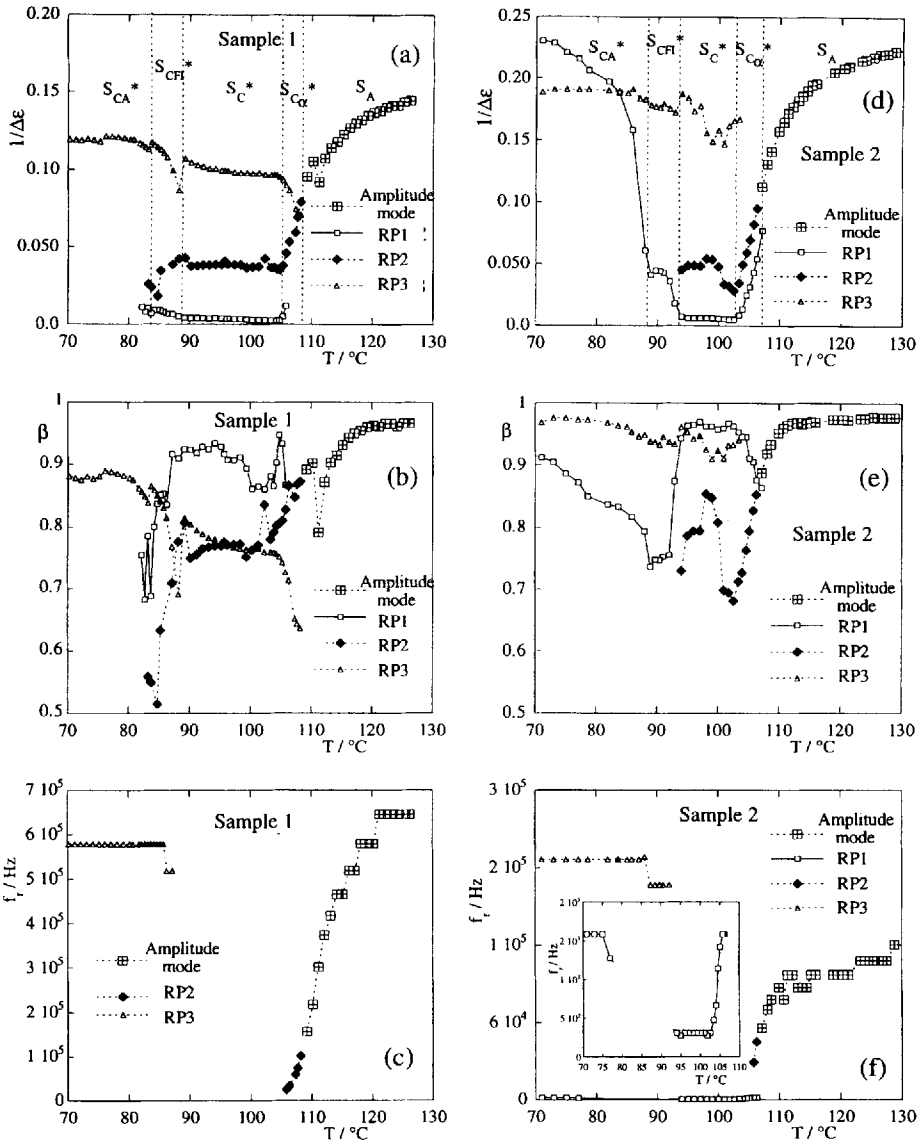

Figure 4. Temperature dependence of $\Delta\varepsilon$, β and f_r (*a*), (*b*), (*c*) for sample 1, and (*d*), (*e*), (*f*) for sample 2. RP1, RP2 and RP3 are relaxation processes occurring at low, intermediate and high frequencies. RP1 corresponds to the Goldstone mode in the $S^*_{C_\alpha}$, S^*_C and $S^*_{C_{FI}}$ phases an to the anti-phase azimuthal mode in the $S^*_{C_A}$ phase. RP2 corresponds to a mode triggered by the amplitude mode and RP3 is associated with the non-collective azimuthal mode.

are very near. The low values of β just above the $S^*_{C_A}$–$S^*_{C_{FI}}$ phase transition (see figures 4 (*b*) and 4 (*e*)) give some support to this idea.

The relaxation process RP3 is detected for the highest frequency range, down below the S_A–$S^*_{C_\alpha}$ transition temperature. The main contribution to the dielectric constant in the low temperature region of the $S^*_{C_A}$ phase comes from this mode (see figures 4 (*a*) and 4 (*d*)). In this phase, ε'' exhibits a clear maximum and f_r is nearly temperature independent. The values of f_r differ for the samples studied, which is probably due to surface interactions.

Recently, Hiraoka *et al.* [8], reported the existence of an azimuthal vibration in the $S^*_{C_A}$ phase of MHPOBC, associated with non-collective distortion of the antiparallel ordering of molecules in neighbouring layers (see figure 6). We suggest that such a vibration can also exist in the $S^*_{C_{FI}}$, S^*_C and $S^*_{C_\alpha}$ phases as a non-collective molecular vibration, changing the azimuthal angle ψ and giving a contribution to the dielectric constant, which we assign to the contribution from RP3.

The plots of the parameter β in figures 4 (*b*) and 4 (*e*)) show, for both samples, a quasi-monodispersive behaviour of the amplitude mode, the Goldstone mode and the

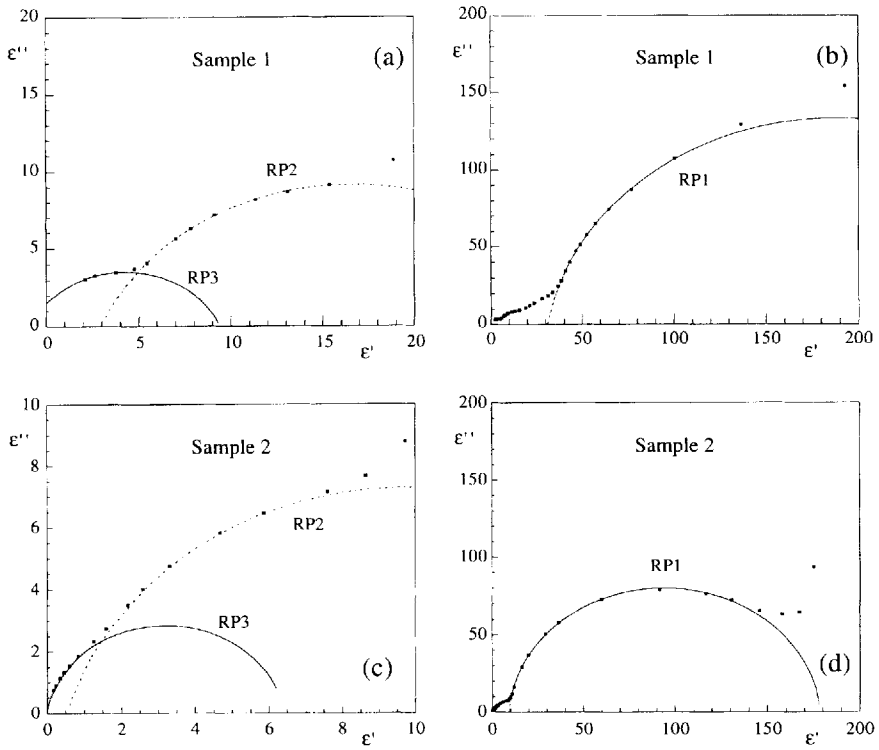

Figure 5. Cole–Cole diagrams at 98°C (S_C^* phase): (*a*), (*b*) for sample 1, and (*c*), (*d*) for sample 2. The lines are Cole–Cole fits to the experimental data (dots in the figure). RP1, RP2 and RP3 are the relaxation processes occurring at low, intermediate and high frequencies.

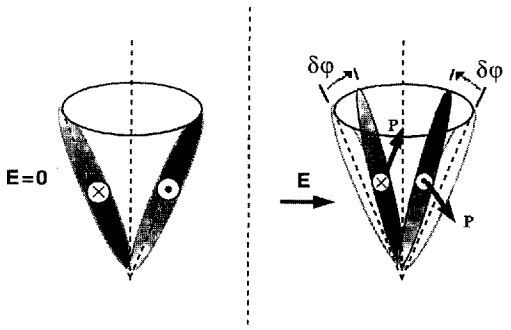

Figure 6. Azimuthal molecular vibration in the $S_{C_A}^*$ phase that contributes to the permittivity [8].

non-collective azimuthal mode in the S_A, S_C^* and the $S_{C_A}^*$ phases, respectively.

In the vicinity of the phase transitions, a polydispersive behaviour is very explicit (β decreases). We must point out that in the $S_{C_{FI}}^*$ and $S_{C_\alpha}^*$ phases none of the identified modes has a monodispersive behaviour, which can be associated with fluctuations of the molecular orientation, competitive phenomena or coexistence of phases.

4. Conclusions

The existence of polar mesophases in the compound studied was confirmed by optical and dielectric measurements.

Five modes were identified as contributing to the dielectric constant. The amplitude (soft) mode, which is responsible for the phase transition to the tilted phases, triggers another relaxation mode that becomes important in the vicinity of the $S_{C_\alpha}^*$–S_C^* phase transition. The Goldstone mode, i.e., the phason mode, gives the strongest contribution to ε' in the $S_{C_\alpha}^*$, S_C^* and $S_{C_{Fi}}^*$ phases. In the antiferroelectric $S_{C_A}^*$ phase the antiparallel molecular order cancels the macroscopic polarization, so that no contribution from the Goldstone mode is observed. In this phase, the only collective mode contributing to the permittivity is the anti-phase azimuthal mode [7].

In all the tilted phases, a non-collective vibration of the molecules changing the azimuthal angle ψ [8] has been detected. In the low temperature range of the $S_{C_A}^*$ phase, the contribution of this non-collective mode becomes the most important contribution to the dielectric constant.

Surface interactions can change the elastic properties of liquid crystalline phases and thus provide different values of f_r and different contributions to the dielectric constant in samples of very different thicknesses. It was shown that these surface interactions cause a thermal hysteresis, especially at the $S^*_{C_A}$–$S^*_{C_{FI}}$ and the $S^*_{C_{FI}}$–S^*_C transition temperatures, as the surface anchoring favours the polar (ferri- or ferro-electric) states relative to the anti-polar (antiferroelectric) state. These effects are more important in thin samples. When the cell thickness increases, the surface effects are attenuated and the liquid crystal begins to reproduce the bulk contributions.

The authors are deeply indebted to Albano Costa for technical assistance, to Dr Manuel Joaquim Marques for helpful discussions about the optical measurements. This work was partially supported by JNICT, by the 'Service Culturel Scientifique et de Coopération de l'Ambassade de France au Portugal', by the 'Instituto Materiais (IMAT-Núcleo IFIMUP)' and by the 'Centro de Física da Universidade do Porto (CFUP)'.

References

[1] Nguyen, H. T., Rouillon, J. C., Cluzeau, P., Sigaud, G., Destrade, C., and Isaert, N., 1994, *Liq. Cryst.*, **17,** 571.
[2] Glogarová, M., Sverenyak, H., Nguyen, H. T., and Destrade, C., 1993, *Ferroelectrics*, **147,** 43.
[3] Destrade, C., Simeão Carvalho, P., and Nguyen, H. T., 1996, *Ferroelectrics*, in press.
[4] Gouda, F, Sharp, K., and Lagerwall, S. T., 1991, *Ferroelectrics*, **113,** 165.
[5] Blinc, R., Copic, M., Drevensek, I., Levstik, A., Musevic, I., and Zeks, B., 1991, *Ferroelectrics*, **113,** 59.
[6] Schacht, J., Gießelmann, F., Zugenmaier, P., and Kuczynski, W., to be published.
[7] Gisse, P., Pavel, J., Nguyen, H. T., and Lorman, V. L., 1993, *Ferroelectrics*, **147,** 27.
[8] Hiraoka, K., Takezoe, H., and Fukuda, A., 1993, *Ferroelectrics*, **147,** 13.